## PAPER

Check for updates

# A numerical study on the interplay between the intra-particle and interparticle characteristics in bimagnetic soft/soft and hard/soft ultrasmall nanoparticle assemblies

Franciscarlos Gomes da Silva, [ID] *[a] Marianna Vasilakaki, [ID] [b] Rafael Cabreira Gomes,[ac] Renata Aquino,[d] Alex Fabiano Cortez Campos, [ID] [d] Emmanuelle Dubois, [ID] [e] Régine Perzynski, [ID] [e] Jérôme Depeyrot[a] and Kalliopi Trohidou [ID] [b]

A mesoscopic scale approach and the Monte Carlo (MC) method have been employed to study the exchange bias behaviour of $MnFe_2O_4$ (soft)/maghemite (soft) and $CoFe_2O_4$ (hard)/maghemite (soft) nanoparticles (NPs) of size $\sim 3$ nm in dense and diluted assemblies at low temperatures. The analysis of our MC results clearly shows that in the powder samples the contribution to the exchange bias field ($H_{ex}$) and the coercivity ($H_c$) comes mainly from the intraparticle core/shell structure in the hard/soft sample and that the interplay between the internal characteristics and the interparticle interactions is more important in the soft/soft samples where the dipolar strength is enhanced. In the diluted frozen ferrofluid samples where interparticle exchange interactions are absent and the role of the dipolar interactions is not significant the exchange bias effects are reduced, and they come from the intra particle structure. The variation of $H_{ex}$ and $H_c$ with the applied cooling field well reproduces the experimental findings and sheds light on the key mechanisms of the observed magnetic behaviour. Our results demonstrate the possibility to control the magnetic behaviour of nanostructures by using properly chosen core/shell bimagnetic nanoparticles.

## 1. Introduction

The exchange bias (EB) effect was discovered in 1956 on Co/CoO core/shell (CS) nanoparticles.[1–3] Later, this effect has been investigated in detail by many research groups from both theoretical[1–4] and experimental[5–9] points of view. The reason for this thorough investigation is that bimagnetic core/shell nanoparticles are becoming progressively more attractive in diverse fields such as hard magnets or magnetic recording media and biomedical applications.[10–12]

In addition, thanks to the progress in controlled chemical synthesis and to the advances in technical instruments for the study of the structural–morphological and magnetic properties, it is possible to explore EB in a wide range of nanoparticle systems, such as doubly inverted nanoparticles,[13,14] core/shell nanoparticles with different compositions,[15,16] and

nanocomposites.[17,18] The experimental results on nanocomposites based on the hexaferrite hard/soft ferrite interface have shown that the magnetic properties depend on the hard/soft phase ratios.[19,20] López-Ortega *et al.* gave a detailed study of the magnetic behaviour and applications of exchange coupled bimagnetic hard/soft and soft/hard magnetic core/shell nanoparticles.[11] In addition, Monte Carlo studies have shed light on the role of interface and surface spins on the exchange bias properties,[1,2,21–23] in various nanoparticle systems.

The cooling field dependence of the exchange bias field and the coercivity in core/shell nanoparticles has been studied by several authors.[2,17,21–26] In these studies, it has been observed that as the applied field increases the exchange bias phenomena are increasing. This is attributed to the competition between the Zeeman energy and the exchange anisotropy energy for a range of applied fields. Further increase of the applied field leads to the reduction of the exchange bias effects because the Zeeman energy starts to dominate and tends to direct the interface spins along the field.

In assemblies of magnetic nanoparticles, interparticle interactions play an important role in the exchange bias behaviour of the systems. It has been demonstrated that the interplay between internal nanoparticle characteristics and interparticle interactions determines the magnetic response of the nanoparticles to an externally applied field.[22,27–29] Indeed, in previous experimental

*aInstituto de Física, Universidade de Brasília, Caixa Postal 04455, 70919-970, Brasília, Brazil. E-mail: franciscarlos@fis.unb.br*

*bInstitute of Nanoscience and Nanotechnology, NCSR "Demokritos", Athens 15310, Greece*

*cDepartamento de Física, Universidade Federal de Santa Catarina, 88040-900, Florianópolis, Brazil*

*dLaboratory for Environmental and Applied Nanoscience, Faculty UnB – Planaltina, University of Brasília, 73345-010, Brasília, Brazil*

*eSorbonne Université, Laboratoire PHENIX, 4 Place Jussieu, Case 51, 75005, Paris, France*

studies, we have investigated the effect of core and shell composition on the exchange bias properties of MnFe$_2$O$_4$@γ-Fe$_2$O$_3$ and CoFe$_2$O$_4$@γ-Fe$_2$O$_3$ core/shell NPs of size $\sim$ 3 nm at low temperature (a few Ks).[24,30–32] By studying dilute and dense dispersions as well as powders, it has been demonstrated experimentally that inter and intraparticle interactions play an important role in the EB properties. Our finding showed that in concentrated frozen dispersions, the dipolar interparticle interaction reduced the exchange bias field. Interparticle exchange bias was found to dominate in powder nanoparticle samples. An open question is the role of the composition and the mechanism of the observed behaviour in MnFe$_2$O$_4$@γ-Fe$_2$O$_3$ (soft/hard) and CoFe$_2$O$_4$@γ-Fe$_2$O$_3$ (hard/soft) nanoparticle systems.

In the present work, we systematically investigate by Monte Carlo simulations the role of the intraparticle characteristics and their interplay with interparticle interactions in the exchange bias behaviour of ferrofluids and powder NPs. These assemblies consisted of complex ultra-small magnetic nanoparticles (of size $\sim$ 3 nm) that can be used for environmental (e.g. increasing magnetoelectric performance[33]) and biomedical applications (e.g. magnetic hyperthermia as nanoheaters[34]).

In particular, the cooling field dependence of $H_c$ and $H_{ex}$ is analysed in dense and in very diluted assemblies (frozen ferrofluids) using mesoscopic scale modelling. Since in the diluted dispersions, interparticle interactions play a minor role the influence of the intraparticle characteristics is clearly revealed. In all cases we discuss the numerical results in the context of our experimental findings.[24,30,31,35,36]

## 2. The model

To model spherical MnFe$_2$O$_4$/γ-Fe$_2$O$_3$ nanoparticle (of diameter $d \sim 3.3$ nm and γ-Fe$_2$O$_3$ shell thickness $t_{sh} = 0.4$ nm) assemblies and spherical CoFe$_2$O$_4$/γ-Fe$_2$O$_3$ nanoparticle (of $d \sim 3.1$ nm and γ-Fe$_2$O$_3$ shell thickness $t_{sh} = 0.5$ nm) assemblies in frozen ferrofluids (very dilute samples) and powders (dense samples), we consider systems of $N$ ultra-small spherical nanoparticles with a ferrimagnetic (FiM) core/FiM shell morphology. We perform the Monte Carlo simulations technique with the

implementation of the Metropolis algorithm to calculate the magnetic behaviour of these assemblies at low temperature $T = 0.01$ in our units which corresponds to 5 K.

The particles are located randomly on the nodes of a cubic lattice inside a box of dimensions $10\alpha \times 10\alpha \times 10\alpha$ for the dense assembly and of dimension $20\alpha \times 20\alpha \times 20\alpha$ for the diluted one, where $\alpha$ is the lattice spacing for the sample and it is equal to the particle diameter $D$, and therefore there is no overlapping of the nanoparticles. It is important to note that the choice of this model is the appropriate one to capture the internal structure and to describe the interparticle characteristics, as discussed in ref. 37.

A set of three classical spin vectors is used to describe each of the nanoparticles in the assembly: one spin for the core $\vec{S}_{ci}$ and two spins $\vec{S}_{sh1i}$ and $\vec{S}_{sh2i}$ for the two sublattices of the shell with magnetic moments $\vec{m}_{\ell,i} = m_{\ell,i}\vec{S}_{\ell,i}$ with $i = 1, ..., N$ and $\ell = $ c, sh1, sh2 and $m_{\ell,i} = M_{s\_\ell,i} \times V_{\ell,i}/M_s \times V$, where $M_{s\_\ell}$ is the saturation magnetization and $V_\ell$ is the volume of each nanoparticle region. $M_s$ is the total saturation magnetization of the nanoparticle and $V$ is the particle volume (Fig. 1). We have considered one spin for the FiM core giving its net magnetic moment with uniaxial anisotropy and two for the shell because of the ultra-small size of the nanoparticle and the very small shell thickness. The two magnetic moments of the shell are randomly oriented. Therefore, in the model, the core is well-ordered retaining some of the bulk characteristics and the shell is disordered, spin-glass like.[22] We introduce short range intraparticle exchange interaction between the Mn or Co ferrite core spin and each of the two maghemite shell spins (interface coupling $J_{c1}$ and $J_{c2}$) and between the two shell spins (shell coupling $J_{shell}$). Long-range inter-particle dipolar interactions among all spins in the assemblies are considered. In the case of the dense assembly (powder sample) for the particles that are in contact, because of the very small shell thickness,[31] the particle core spin interacts with the nearest neighbor shell spins via exchange interactions ($J_{csh1}, J_{csh2}$).[37] The shell spins of the nearest neighbours are also exchange coupled ($J_{sh1sh2}$).

The total energy of the system for the $N$ nanoparticles is given by:

$$
\begin{aligned}
E = &-\frac{1}{2}\sum_{i=1}^{N}\left[J_{c1}\left(\vec{S}_{c,i}\cdot\vec{S}_{sh1,i}\right) + J_{c2}\left(\vec{S}_{c,i}\cdot\vec{S}_{sh2,i}\right) + J_{shell}\left(\vec{S}_{sh1,i}\cdot\vec{S}_{sh2,i}\right)\right] \\
&-K_c\sum_{i=1}^{N}\left(\vec{S}_{c,i}\cdot\hat{e}_{c,i}\right)^2 - K_{sh}\sum_{i=1}^{N}\left[\left(\vec{S}_{sh1,i}\cdot\hat{e}_{sh1,i}\right)^2 + \left(\vec{S}_{sh2,i}\cdot\hat{e}_{sh2,i}\right)^2\right] \\
&-\mu_0 H\sum_{i=1}^{N}\left(m_{c,i}\vec{S}_{c,i} + m_{sh1,i}\vec{S}_{sh1,i} + m_{sh2,i}\vec{S}_{sh2,i}\right)\cdot\hat{e}_h \\
&-\frac{1}{2}g\sum_{\substack{i,j=1 \\ i\neq j}}^{N}\left(m_{c,i}\vec{S}_{c,i} + m_{sh1,i}\vec{S}_{sh1,i} + m_{sh2,i}\vec{S}_{sh2,i}\right)D_{ij}\left(m_{c,j}\vec{S}_{c,j} + m_{sh1,j}\vec{S}_{sh1,j} + m_{sh2,j}\vec{S}_{sh2,j}\right) \\
&-\frac{1}{2}\sum_{\langle i,j\rangle}^{N}\left[J_{sh1sh2}\left(\vec{S}_{sh1,i}\cdot\vec{S}_{sh2,i}\right) + J_{csh1}\left(\vec{S}_{c,i}\cdot\vec{S}_{sh1,j}\right) + J_{csh2}\left(\vec{S}_{c,i}\cdot\vec{S}_{sh2,j}\right)\right]
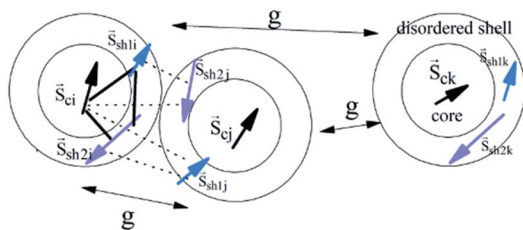\end{aligned}
\tag{1}
$$

Fig. 1 Schematic representation of the intra-particle and the inter-particle interactions of three random particles ($i$, $j$, and $k$) in the assembly. The solid lines show the exchange intra-particle and the broken lines the exchange inter-particle (when the nanoparticles are in contact) interactions respectively. The double arrows show the dipolar inter-particle interactions of dipolar strength $g$. Note that the random orientation of the shell spins effectively describes the disordered shell.

In eqn (1), the first three energy terms inside the brackets describe the intra-particle Heisenberg exchange interaction between the spins in each nanoparticle, the core (c) with shell spin1 (sh1), the core with shell spin2 (sh2) and between the shell spins respectively. The fourth and the fifth terms give the anisotropy energy of the core and the shell spins ($\hat{e}_i$ is the random anisotropy easy-axis direction), respectively. The sixth term is the Zeeman energy ($\hat{e}_h$ is the direction of the magnetic field). The next term gives the dipolar interactions among all the spins in the assembly, where $D_{ij}$ is the dipolar interaction tensor which in our case takes the values of the Ewald matrix.[37]

The last three terms exist only in the case of the powder sample and describe the inter-particle exchange interactions between the neighboring shells and between the core of each nanoparticle with the neighboring shell spins respectively. There is no exchange interparticle term in the frozen ferrofluid sample.

The dipolar strength is $g = \mu_0(M_sV)^2/4\pi d^3$, where $d$ is the diameter of the particle. The anisotropy constant of the core is $K_c$ and of the shell $K_{sh}$, the external magnetic field is $\mu_0H$ and the thermal energy is $k_BT$ (where $T$ is the temperature). The particle volume concentration $\varphi$ is taken as 27% for the powder samples and 0.4% for the frozen ferrofluids.

The magnetic moments of the core and of the shell are extracted from an atomic scale model of the spinel ferrite structure that explicitly takes into account the size of the shell and the core of the $MnFe_2O_4/\gamma\text{-}Fe_2O_3$ and $CoFe_2O_4/\gamma\text{-}Fe_2O_3$ nanoparticles and calculates their volumes and their saturation magnetization.

In the $MnFe_2O_4/\gamma\text{-}Fe_2O_3$ nanoparticle (of size $d \sim 3.3$ nm) assemblies, the energy parameters are normalized by the volume anisotropy of the shell $K_{sh} \times V_{sh}$ so they are dimensionless. The normalized magnetic moments are: $m_c = 0.15$ for the core and $m_{sh1} = 0.50$ and $m_{sh2} = 0.58$ for the shell. In this atomic scale model, the saturation magnetization has been taken 1.5 times higher than the core magnetization in agreement with the experimental results of ref. 32 ($M_{score} = 210$ kA m$^{-1}$ and $M_s = 320$ kA m$^{-1}$). We consider the bulk value of $MnFe_2O_4$ for the core anisotropy ($K_c = 3 \times 10^3$ J m$^{-3}$) and the shell anisotropy $\sim 10$ times higher than the bulk maghemite anisotropy ($K_c = 5 \times 10^3$ J m$^{-3}$). The reduced parameters

entered into our simulations for the anisotropy strength are for the core $K_c = 0.04$ and for the shell $K_{sh} = 1.0$. Our atomic scale simulations show that in the core the B sublattice is the dominant one, therefore we set the core macrospin as a "B" spin. For the intraparticle exchange coupling constant strengths between the core spin and the shell spins of the two sublattices A and B we use their bulk values for the $MnFe_2O_4$ ($J_{AB} = -22.7$ K and $J_{BB} = 11.5$ K, $s_A = s_B = 5/2$) spinel structure and the exchange coupling constants of the maghemite ($J_{AB} = -25.9$ K and $J_{BB} = 12.7$ K, $s_A = s_B = 5/2$) spinel structures. From the atomic scale modeling the exchange coupling constant between the A and B shell spins is found to be 1.44 times larger than the corresponding core value and by rescaling them we find that $J_{c1} = -1.6$, $J_{c2} = 0.8$, and $J_{shell} = -2.3$. There is no exact microscopic model for the calculation of the exchange coupling constant strengths between the nanoparticles, and thus we consider the inter-particle exchange interactions between the shell spins of particles in contact with the $J_{AB}$ of the bulk maghemite and in our model the rescaled value is $J_{sh1sh2} = -0.5$. The values of the core spins with the neighboring shell spins are $J_{csh1} = 0.15$ and $J_{csh2} = -0.18$. From the experimental values of $M_s = 320$ kA m$^{-1}$ for the dilute sample with $\varphi = 0.4\%$, the dipolar strength is found to be $g = 0.16$. In the powder sample the experimental hysteresis loop gives enhanced saturation magnetization by a factor of 1.095 compared to the frozen ferrofluid samples. This increase in the magnetization in the dense sample is attributed to the inter-particle exchange interactions between the particles in contact. Therefore, for the powder samples we find that $g = 0.16 \times 1.2 = 0.19$.

The energy parameters of the $CoFe_2O_4/\gamma\text{-}Fe_2O_3$ nanoparticles (of $d \sim 3.1$ nm) are also normalized by the factor $K_{sh} \times V_{sh}$ used in the previous system, so that we can compare the two types of samples. In this case, from our experimental findings we have found that the $CoFe_2O_4$ core magnetization is lower ($\sim 5\%$) than that of the $MnFe_2O_4$ core and thus the normalized magnetic moment of this core is taken as $m_c = 0.14$. We take $m_{sh1} = 0.15$ and $m_{sh2} = 0.8$ for the maghemite shell since its volume size ($t_{sh} = 0.5$ nm) and the pinning parameter ($p = 0.03$) are larger than those of the shell of the $MnFe_2O_4/\gamma\text{-}Fe_2O_3$ nanoparticles ($t_{sh} = 0.4$ nm and $p = 0.01$) in agreement with the experimental results. The bulk exchange coupling constant strengths of $CoFe_2O_4$ are $J_{AB} = -25$ K $J_{BB} = 18$ K, $s_A = 5/2$, and $s_B = 2$, and using these values in our atomic scale model we find that $J_{c1} = -1.76$, $J_{c2} = 1.25$, and $J_{shell} = -2.87$. The interparticle exchange coupling strengths between the core spins and the neighboring shell spins in the $CoFe_2O_4/\gamma\text{-}Fe_2O_3$ nanoparticle systems are $J_{csh1} = 0.165$ and $J_{csh2} = -0.28$. The value of the exchange coupling constant between the shell spins of nanoparticles in contact as above is taken from the $J_{AB}$ bulk value of maghemite and in our model this becomes $J_{sh1sh2} = -0.62$. These interparticle exchange constant values are lower than the intra-particle ones ($\sim 10$, 4, and 5 times respectively as in the system of $MnFe_2O_4/\gamma\text{-}Fe_2O_3$ nanoparticles).

In ref. 28, it has been demonstrated that the anisotropy field of the $CoFe_2O_4/\gamma\text{-}Fe_2O_3$ assembly is 3 times larger than the anisotropy field of $MnFe_2O_4/\gamma\text{-}Fe_2O_3$ as it was estimated from the virgin magnetization curves of both systems. Therefore, if

we consider that the core anisotropy has the bulk value $K_c = 2 \times 10^5$ J m$^{-3}$ for CoFe$_2$O$_4$, the increase in the effective anisotropy of the system comes from the shell. Therefore, the shell anisotropy is three times larger than that of the MnFe$_2$O$_4$/γ-Fe$_2$O$_4$ system. So, the anisotropy strengths are $K_c = 1.6$ for the core and $K_{sh} = 3.0$ for the shell. The dipolar strength of the frozen ferrofluid sample is found to be $g = 0.034$, much smaller than that of the MnFe$_2$O$_4$/γ-Fe$_2$O$_3$ assemblies, due to the smaller $M_s = 160$ kA m$^{-1}$ as estimated from the experimental hysteresis loop. In the powder samples, assuming the same enhancement of the saturation magnetization as in MnFe$_2$O$_4$/γ-Fe$_2$O$_3$ nanoparticles assemblies, we find $g = 0.041$ larger by a factor of 1.2.

There is experimental evidence that all the nanoparticle assemblies are polydisperse following a log-normal distribution. Therefore, by introducing in our model the same particle volume polydispersity, we recalculate the corresponding volume dependent parameters, namely the magnetizations $m_c$, $m_{sh1}$, and $m_{sh2}$ and the anisotropies $K_c$ and $K_{sh}$ for each nanoparticle of the polydisperse assembly.

## 3. Results and discussion

Fig. 2 shows the experimental results on the cooling field dependence of the exchange bias field $H_{ex}$ (Fig. 2(a and b)) together with the data of the Monte Carlo simulations (Fig. 2(c and d)) for frozen ferrofluid (0.4%) (open symbols) and powders (closed symbols) of the MnFe$_2$O$_4$@γ-Fe$_2$O$_3$ (Fig. 2(a and c)) and CoFe$_2$O$_4$@γ-Fe$_2$O$_3$ (Fig. 2(b and d)) core/shell nanoparticles respectively. In all simulations, the particle size polydispersity is included.

The calculated curves (Fig. 2(c and d)) of the cooling field dependence of $H_{ex}$ show a maximum (peak) in both samples in agreement with the experimental findings (Fig. 2(a and b)). The
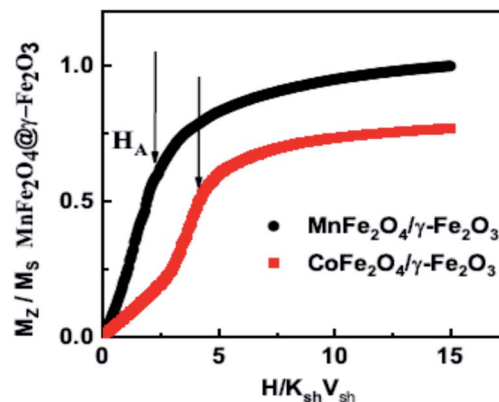
Fig. 3 Calculated virgin magnetization curves for powder samples of CoFe$_2$O$_4$@γ-Fe$_2$O$_3$ and MnFe$_2$O$_4$@γ-Fe$_2$O$_3$ core/shell nanoparticles. The arrows indicate the position of the anisotropy field in both samples.

peak position is located at $H_{cool}/K_{sh}V_{sh} \sim 1.5$ and $\sim 3.5$ for MnFe$_2$O$_4$@γ-Fe$_2$O$_3$ and CoFe$_2$O$_4$@γ-Fe$_2$O$_3$ core/shell nanoparticles, respectively. These values are close to the half of the anisotropy fields given by $H_a/K_{sh}V_{sh} \sim 3$ and $H_a/K_{sh}V_{sh} \sim 5$ as is estimated from the calculated virgin curves of powder samples (see Fig. 3) in qualitative agreement with the experimental results.[31,36] We must note here that the deviation is due to the structural difference between the experimental situation and the model. In the case of dilute dispersions (almost isolated particles) both the MC results and the experimental measurements show that the maximum of $H_{ex}$ is smaller than in powder. Moreover, the value of $H_{ex}$ maximum is more than two times larger for the CoFe$_2$O$_4$@γ-Fe$_2$O$_3$ sample than for the MnFe$_2$O$_4$@γ-Fe$_2$O$_3$ one. This result has been attributed to a stronger pinning of the more anisotropic cores in ref. 31 and indicates that the shell spin pinning through the core/shell interface depends on the hardness of the core ferrite.[31]

Monte Carlo simulation findings indeed give larger $H_{ex}$ values for CoFe$_2$O$_4$@γ-Fe$_2$O$_3$ core/shell nanoparticles in good agreement with the experimental results. For both types of samples, the measured values of $H_{ex}$ are found to be larger in powders than in the diluted frozen dispersions for all the investigated range of cooling fields. This has been attributed to a collective interparticle exchange interaction acting through the multi-connected shells, which are in contact with powder samples, and are behaving as a spin glass-like matrix where the FI cores are embedded.[36,38] As can be seen in Fig. 2(c and d) Monte Carlo simulation data well reproduce this feature. This will be further illustrated in the discussion below where we separately study the contribution from the dipolar and exchange interparticle interactions.

The simulation results also confirm that the interface interaction between the Co ferrite core and the spin-glass like maghemite shell, which is the origin of the $H_{ex}$, is rather insensitive to interparticle interactions. For CoFe$_2$O$_4$@γ-Fe$_2$O$_3$ nanoparticles, the ratio of the maximum $H_{ex}$ values in both the powder and the diluted frozen liquid samples is indeed 1.3 (close to the experimental ratio of 1.4) and is smaller than the
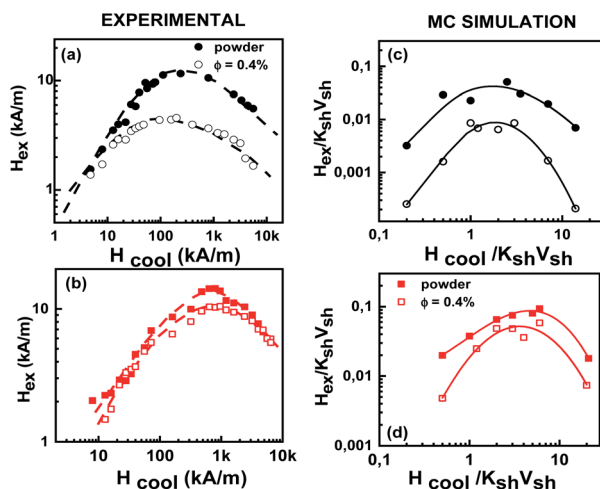
Fig. 2 Cooling field dependence of the exchange bias field $H_{ex}$ extracted from hysteresis loops. Experimental data on the left panel (a and b) are compared with the Monte Carlo simulations results on the right panel (c and d) for frozen ferrofluid (open symbols) and a powder (full symbols) for the MnFe$_2$O$_4$@γ-Fe$_2$O$_3$ (a and c) and CoFe$_2$O$_4$@γ-Fe$_2$O$_3$ (b and d) core/shell nanoparticles respectively. The dashed and solid lines are guides to the eye.

corresponding value found for MnFe$_2$O$_4$@ γ-Fe$_2$O$_3$ core/shell nanoparticles in agreement with the experimental findings.

Fig. 4 illustrates the cooling field dependence of the coercivity $H_c$ as deduced from the hysteresis loops after field cooling. Experimental data (Fig. 4(a and b)) are compared with those obtained from Monte Carlo simulations (Fig. 4(c and d)) for frozen ferrofluid (0.4%) (open symbols) and powder (closed symbols) of MnFe$_2$O$_4$@γ-Fe$_2$O$_3$ (upper panel) and CoFe$_2$-O$_4$@γ-Fe$_2$O$_3$ (lower panel) core/shell nanoparticles.

The observed behaviour is slightly different in the two types of core/shell nanoparticle samples. The coercivity of MnFe$_2$-O$_4$@γ-Fe$_2$O$_3$ core/shell nanoparticles does not vary within the studied cooling field range, whereas the $H_c$ curves obtained for CoFe$_2$O$_4$@γ-Fe$_2$O$_3$ core/shell nanoparticles exhibit a small increase (4–5%) in a broad range of high cooling field values (0.6–3 × 10$^3$ kA m$^{-1}$). These experimental findings (Fig. 4(a and b)) are well reproduced by Monte Carlo simulations (Fig. 4(c and d)). Also, in agreement with the experimental results, for MnFe$_2$O$_4$@γ-Fe$_2$O$_3$ core shell nanoparticles, the calculations show that the coercivity of the frozen liquid samples is more than 2 times smaller than that of the powder ones.

In order to further investigate the contribution of the interparticle interactions, the intraparticle characteristics and their interplay in the observed magnetic behaviour, MC simulations are performed for very diluted frozen ferrofluids (almost non-interacting $J_{inter} = J_{sh1sh2} = J_{csh1} = J_{csh2} = 0.0$), where we: (a) switch off the dipolar interactions ($g = 0$) or (b) the shell anisotropy is taken equal to the core one (setting $K_{sh} = K_c$) or (c) we set both ($K_{sh} = K_c$ and $g = 0$). In addition, in dense nanoparticle assemblies (powder samples) we also switch off either (c) the exchange interparticle interaction ($J_{inter} = 0$) or (d) all the interparticle interactions ($g = J_{inter} = 0$). Fig. 2 and 4 illustrate the behaviour of the exchange bias field and the coercivity as a function of the cooling field respectively, for the powder samples (a–d) and the frozen diluted ferrofluids (e and f) of the

MnFe$_2$O$_4$@γ-Fe$_2$O$_3$ (upper panel) and CoFe$_2$O$_4$@γ-Fe$_2$O$_3$ (lower panel) CS nanoparticles.

In Fig. 5(a, b) and 6(a and b), the results of $H_{ex}$ and $H_c$ vs. the cooling field for $g = 0$ (closed stars), $J_{inter} = 0$ (up triangles) and $g = J_{inter} = 0$ (down triangles) are compared with the full models MnFe$_2$O$_4$@γ-Fe$_2$O$_3$ and CoFe$_2$O$_4$@γ-Fe$_2$O$_3$ (full circles). In Fig. 5(c, d) and 6(c and d), the $H_{ex}$ and $H_c$ vs. the cooling field results for $K_{sh} = K_c$ (open circles), $K_{sh} = K_c$ and $g = 0$ (open stars), $K_{sh} = K_c$ and $J_{inter} = 0$ (open up triangles) are presented. Finally, in Fig. 5(e, f), 6(e and f) the cases of diluted frozen ferrofluids with $g = 0$ (closed stars), $K_{sh} = K_c$ (open circles) and $K_{sh} = K_c$ and $g = 0$ (open stars) are compared with the full models MnFe$_2$O$_4$@γ-Fe$_2$O$_3$ and CoFe$_2$O$_4$@γ-Fe$_2$O$_3$ (full circles).

In MnFe$_2$O$_4$@γ-Fe$_2$O$_3$ powders (Fig. 5(a and c)), $H_{ex}$ depends significantly on the dipolar interactions because they have a large dipolar strength compared to the anisotropy strength. The role of the intraparticle interface is not significant because of the low $K_c$ (25 times smaller than $K_{sh}$); therefore the shell with the higher $k$ is dragging the core spin. For the maximum of the $H_{ex}$ curve, they are close to the field where the Zeeman energy competes with the shell anisotropy (because this gives the dominant contribution) and the anisotropy induced by the dipolar interactions. On the other hand, in the CoFe$_2$O$_4$@γ-Fe$_2$O$_3$ powders, Fig. 6(b and d) shows that the exchange bias mainly comes from the intraparticle interface (core/shell) and from the competition between neighbouring shells due to the interparticle exchange interactions. However, the dipolar interaction does not significantly influence the intensity of the exchange bias field Fig. 5(b) (stars). The maximum $H_{ex}$ is in the field region where the Zeeman energy competes with the shell anisotropy energy. Then when the Zeeman energy overcomes the shell anisotropy energy the spins start to align towards the field and the $H_{ex}$ gradually reduces.

In the frozen diluted ferrofluids shown in Fig. 5(e and f) the role of dipolar interaction is not very significant because of the low concentration. In this case, the role of $J_{inter}$ is negligible. Moreover, if we set $K_{sh} = K_c$ in both types of nanoparticles the EB field is at least one order of magnitude lower. This does
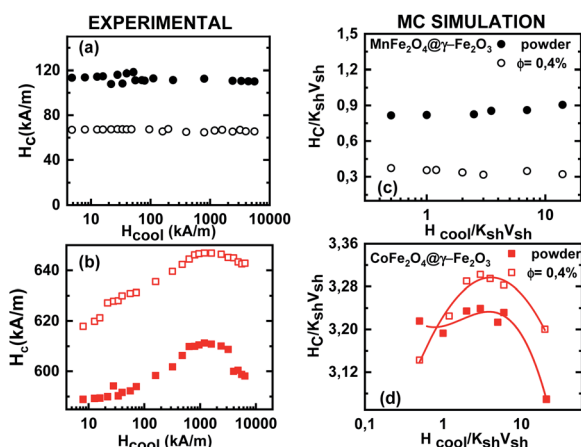


**Fig. 4** Cooling field dependence of the coercivity $H_c$ The experimental data (a and b) are compared with the Monte Carlo simulations results (c and d) for frozen ferrofluid (open symbols) and powder (full symbols) of the MnFe$_2$O$_4$@γ-Fe$_2$O$_3$ (a and c) and CoFe$_2$O$_4$@γ-Fe$_2$O$_3$ (b and d) core/shell nanoparticles respectively. The solid lines are guides to the eye.
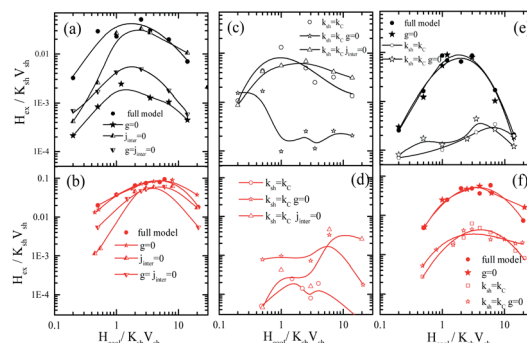


**Fig. 5** Monte Carlo results of the cooling field dependence of the exchange bias field $H_{ex}$ for different values of the simulations parameters for the simulated powder samples. (a–d) And the diluted frozen ferrofluids (e and f) of the MnFe$_2$O$_4$@γ-Fe$_2$O$_3$ (upper panel) and the CoFe$_2$O$_4$@γ-Fe$_2$O$_3$ (lower panel) CS nanoparticles. The solid lines are guides to the eye.
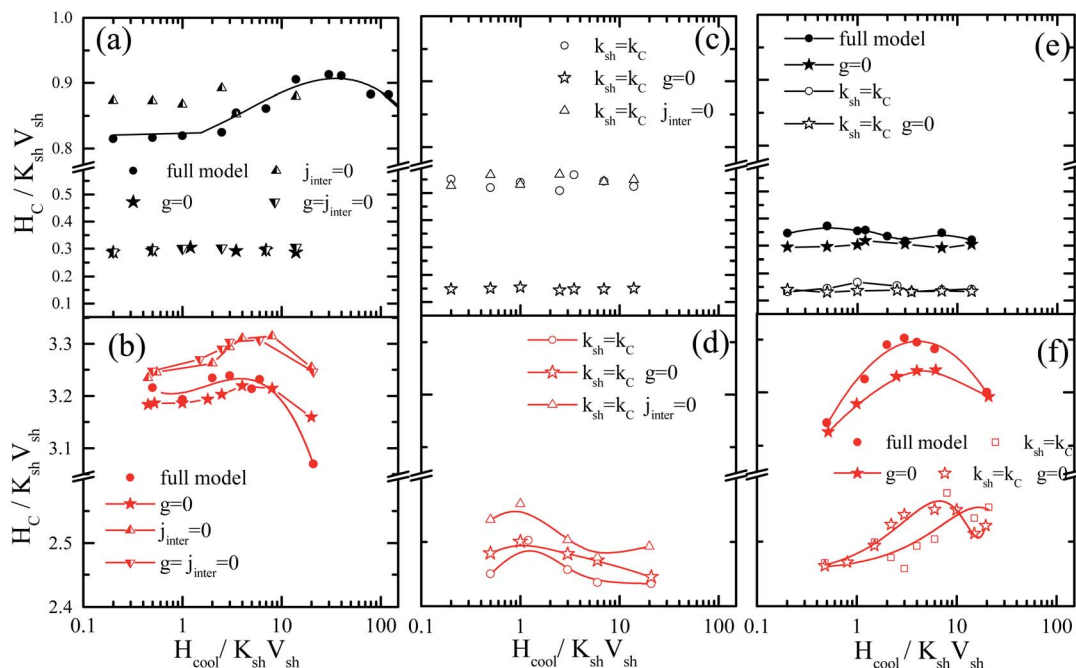
**Fig. 6** Monte Carlo results of the cooling field dependence of the coercivity $H_c$ for different values of the simulations parameters, for powder samples (a–d) and diluted frozen ferrofluids (e and f) of $MnFe_2O_4@\gamma\text{-}Fe_2O_3$ (upper panel) and $CoFe_2O_4@\gamma\text{-}Fe_2O_3$ (lower panel) CS nanoparticles. The solid lines are guides to the eye.

**Table 1** Characteristics of the core−shell NPs[a]

| Core–shell NPs | $d$ (nm) | $t_{sh}$ (nm) | $H_a$ (kA m$^{-1}$) | $p$ |
|---|---|---|---|---|
| $MnFe_2O_4@\gamma Fe_2O_3$ | 3.3 | 0.4 | $4 \times 10^2$ | 0.01 |
| $CoFe_2O_4@\gamma Fe_2O_3$ | 3.1 | 0.5 | $1.2 \times 10^3$ | 0.03 |

[a] $d$: mean crystalline NP diameter deduced from powder X-ray diffraction; $t_{sh}$: shell thickness deduced from chemical titrations; $H_a$: anisotropy field deduced from the first magnetization curve obtained at 5 K in ref. 31; $p$: NPs surface pinning parameter as deduced in ref. 31.

suggest that the anisotropy contrast at the interface between core and shell materials is one of the key parameters that govern exchange bias behaviour. In the case of the hard core the interface competition is stronger, in good agreement with experimental findings that show a larger bias for $CoFe_2O_4@\gamma\text{-}Fe_2O_3$ CS nanoparticles.

Fig. 6 shows the coercivity as a function of the cooling field, for the simulated powder samples (a–d) and the frozen ferrofluids (e and f) of $MnFe_2O_4@\gamma\text{-}Fe_2O_3$ (upper panel) and $CoFe_2O_4@\gamma\text{-}Fe_2O_3$ (lower panel) CS nanoparticles.

In the powder assembly of manganese ferrite/maghemite nanoparticles (Fig. 6(a and c)), the strong character of the dipolar strength that induces a strong anisotropy results in the observed large $H_c$ and when they are switched off ($g = 0$ closed stars) the $H_c$ drastically reduces, as seen in Fig. 6(a). On the other hand, the absence of interparticle exchange interactions ($J_{inter} = 0$ up triangles) results in a small increase in $H_c$. It is important to note that the absence of cooling field dependence of $H_c$ in the experimentally studied cooling field range (in Fig. 4(a)) is due to the fact that the contribution from both shell

anisotropy and dipolar interactions require a higher cooling field to compete with. Therefore, we expect the maximum to appear at a field higher than that available for the measurements. Indeed, this is the situation in Fig. 6(a) (full circles) where coercivity $H_c$ versus the cooling field plot is shown for a more extended cooling field range. For higher cooling field values the curve is reduced after a maximum.

In cobalt ferrite based nanoparticle samples (Fig. 6(b, d and f)), $H_c$ has a maximum value near the point that the Zeeman energy competes with the shell anisotropy energy. Then, it reduces for the same reason as in the $H_{ex}$ variations (Zeeman coupling of disordered shell spins). In the case of powder assembly, the dipolar strength is small; therefore it does not have significant influence on the $H_c$ (Fig. 6(b), stars). Because of the high density of the assembly (powder), the dipolar interactions induce an extra anisotropy (nose to tail dipoles) and when they are switched off the coercivity $H_c$ reduces. On the other hand, the absence of $J_{inter}$ enhances $H_c$ (up triangles or down triangles) because of the non-coherent rotation of the neighbouring spins. Therefore, the more significant contribution in both $H_c$ and $H_{ex}$ comes from the intraparticle structure and in particular from the interplay of the particle shell anisotropy with the interparticle interactions. This can be clearly seen if we set $K_{sh} = K_c$ eliminating the shell anisotropy contribution either with (Fig. 6(d) open circles) or without interparticle interactions (Fig. 6(d) open triangles and open stars).

For the frozen diluted ferrofluid samples the influence of dipolar interactions on $H_c$ is not significant due to the low concentration of magnetic CS nanoparticles. Their absence results in a decrease in $H_c$ (Fig. 6(e and f) closed stars). Finally, if the shell anisotropy is taken to be equal to the core one ($K_{sh} =$

$K_c$) evidently the coercivity $H_c$ decreases in both $MnFe_2O_4$ and $CoFe_2O_4$ based CS nanoparticles (Fig. 6(e and f) open symbols).

# 4. Conclusions

We have employed a mesoscopic scale approach to study the low temperature hysteresis behaviour of soft/soft and hard/soft ultra-small bimagnetic nanoparticles composed of a $MnFe_2O_4$ or $CoFe_2O_4$ core surrounded by a thin maghemite shell. A dense assembly and a very diluted ferrofluid are considered for both types of nanoparticles. In all cases, inter-particle and intra-particle interactions together with particle size polydispersity are included in our studies. Our numerical results are given together with the experimental results and interpret the observed experimental behaviour.

Our results show that the cooling field dependence of the $H_{ex}$ is non-monotonic for both diluted and dense assemblies. The $H_{ex}$ is higher for the dense assemblies of bimagnetic nanoparticles due to the collective interparticle exchange interactions acting through the multi-connected shells. The maximum exchange bias field appears at a cooling field value equal to half the corresponding anisotropy field as indicated by the virgin curves. On the other hand, the coercive field does not vary significantly in a broad range of cooling fields for the soft/soft nanoparticle assemblies, and it is larger in the case of the dense assemblies as expected due to the enhanced inter-particle interactions. Surprisingly, the above $H_c$ behaviour is different for the hard/soft assemblies where the coercive field takes higher values in the case of diluted ferrofluids and exhibits a peak at higher cooling field values for both dense and diluted assemblies attributed to the large anisotropy of particles. This variation of $H_{ex}$ and $H_c$ with the applied cooling field is in good qualitative agreement with the experimental findings.

The overall analysis of our results clearly demonstrates that the more significant contribution to $H_{ex}$ and $H_c$ of the $CoFe_2O_4@\gamma$-$Fe_2O_3$ nanoparticles comes from the intraparticle structure with the interparticle interactions playing a minor role in both ferrofluids and powders. The interplay is much stronger in manganese ferrite/maghemite nanoparticle dense assemblies where the dipolar interactions play the dominant role, because of their larger contribution compared to the particles anisotropy. In the diluted ferrofluids, the dipolar contribution is not significant because of the low particle concentration.

Our results demonstrate the possibility to control the magnetic behaviour of nanostructures by using appropriate core/shell bimagnetic nanoparticles.

# 5. Experimental section

## 5.1 NP synthesis and XRD characterization

The synthesis and characterization of the $MnFe_2O_4@\gamma Fe_2O_3$ or $CoFe_2O_4@\gamma Fe_2O_3$ core–shell NPs, probed here either in dilute colloidal dispersions or in powders, have been extensively described in ref. 31. We recall here the main important aspects.

The very small NPs are obtained by coprecipitation of stoichiometric aqueous solutions of divalent metals $X^{2+}$ ($X^{2+}$ is either $Mn^{2+}$ or $Co^{2+}$) and $Fe^{3+}$ ions in a $NH_3$ buffer at pH 11, under vigorous stirring at 100 °C.[39] In order to reduce the concentrations of free ions in the solution and to clean the particle surfaces, the precipitate is washed with a 2 mol l$^{-1}$ aqueous $HNO_3$ solution. A hydrothermal treatment of the NPs with a $Fe(NO_3)_3$ solution at 100 °C produces a thin maghemite ($\gamma$-$Fe_2O_3$) shell around the core of $XFe_2O_4$. This shell avoids chemical degradation of the core in an acidic medium and tunes the chemical stability of NPs. Its thickness $t_{sh}$ (see Table 1) is obtained by chemical titration.[40] This maghemite shell also imparts the NPs with an electrostatic superficial charge, allowing their stable dispersion in aqueous media at room temperature.[40]

Powder X-ray diffraction experiments at the Brazilian Synchrotron Light Laboratory-LNLS confirm the spinel structure of the NPs. The Scherrer equation applied to the [311] most intense line of the diffractograms allows the deduction of the mean crystalline NP diameter $d$, given in Table 1. The roughly spherical shape and the size distribution of the NPs were also investigated by transmission electron microscopy (TEM) at UPMC-Paris 6 with a JEOL JEM-100 CX II microscope.[31]

## 5.2 Magnetic measurements

DC magnetization measurements are performed at low temperature using a PPMS (Physical Property Measurement System) from UnB and SU with a Vibrating Sample Magnetometer set-up. Their superconducting coil produces magnetic fields in the range of $7.7 \times 10^4$ kA m$^{-1}$, down to a temperature of $T = 2$ K. The magnetic field dependence of the magnetization is measured either in zero-field-cooled (ZFC) and or in field-cooled (FC) modes, for the latter in progressive increasing fields.

For the investigation of the coupling between the NP cores and their disordered surface spins, we mainly focus here on the study of the FC magnetic hysteresis loops. The samples are first frozen in a zero field, down to $T = 250$ K (below the temperature of solvent freezing) to avoid any sample texture, both for dilute dispersions and for powders, of respective NP volume fractions of 0.4% and 27%. This procedure ensures that, in all the measurements carried out, the same spatial organization and randomness of the magnetic anisotropy axis of the various NPs takes place. A static magnetic field is then applied while the temperature is decreased from 250 K down to low temperature, and after this field cooling process the magnetic hysteresis is recorded. Between two loop measurements the temperature is increased back to 250 K, far above the NP blocking temperature.[31] For more details on the magnetic measurement procedures see ref. 31.

Single particle behaviours, averaged over the assembly, are observed in frozen dilute dispersions, as the NPs are far away from each other, without contact. In contrast in powders, NPs are in direct contact and collective behaviours can be observed.[36]

The loops are observed to be $H$-shifted along negative fields, in FC measurements. The exchange bias ($H_{ex}$) and the coercive field ($H_c$) are then quantified by the following relations:

$$H_{ex} = (H_c^+ + H_c^-)/2 \qquad (2)$$

$$H_c = (H_c^+ - H_c^-)/2 \qquad (3)$$

where $H_c^+$ and $H_c^-$ are the fields at which the loop intersects the field axis. It is checked that no "minor-loop" effects are observed in these experiments.[31]

## Author contributions

Franciscarlos Gomes da Silva: conceptualization, methodology, data curation, resources, writing—original draft, writing—review & editing. Marianna Vasilakaki: conceptualization, theoretical model, methodology, writing—review & editing. Rafael Cabreira Gomes: conceptualization, methodology, data curation, validation. Renata Aquino: sample preparation, methodology, data curation. Alex Fabiano Cortez Campos: methodology, writing—review & editing. Emmanuelle Dubois: methodology, writing—review & editing. Régine Perzynski: conceptualization, methodology, resources, writing—review & editing. Jérôme Depeyrot: conceptualization, methodology, resources, writing—original draft, writing—review & editing. Kalliopi Trohidou: conceptualization, theoretical model, methodology, writing—review & editing.

## Conflicts of interest

There are no conflicts to declare.

## Acknowledgements

## References

1 E. Eftaxias and K. N. Trohidou, *Phys. Rev. B: Condens. Matter Mater. Phys.*, 2005, **71**, 134406.

2 M. Vasilakaki and K. N. Trohidou, *Phys. Rev. B: Condens. Matter Mater. Phys.*, 2009, **79**, 144402.

3 Y. Hu, Y. Liu and A. Du, *J. Magn. Magn. Mater.*, 2011, **323**, 2613–2621.

4 S. P. Tsopoe, C. Borgohain, R. Fopase, L. M. Pandey and J. P. Borah, *Sci. Rep.*, 2020, **10**, 18666.

5 R. Skomski and J. M. D. Coey, *Phys. Rev. B: Condens. Matter Mater. Phys.*, 1993, **48**, 15812–15816.

6 H. Khurshid, M.-H. Phan, P. Mukherjee and H. Srikanth, *Appl. Phys. Lett.*, 2014, **104**, 072407.

7 L. del Bianco, A. Hernando, M. Multigner, C. Prados, J. C. Sánchez-López, A. Fernández, C. F. Conde and A. Conde, *J. Appl. Phys.*, 1998, **84**, 2189–2192.

8 G. C. Lavorato, E. Lima, H. E. Troiani, R. D. Zysler and E. L. Winkler, *Nanoscale*, 2017, **9**, 10240–10247.

9 D. Das and A. Alam, *Phys. Rev. Mater.*, 2021, **5**, 044404.

10 V. Skumryev, S. Stoyanov, Y. Zhang, G. Hadjipanayis, D. Givord and J. Nogués, *Nature*, 2003, **423**, 850–853.

11 A. López-Ortega, M. Estrader, G. Salazar-Alvarez, A. G. Roca and J. Nogués, *Phys. Rep.*, 2015, **553**, 1–32.

12 S. Noh, S. H. Moon, T.-H. Shin, Y. Lim and J. Cheon, *Nano Today*, 2017, **13**, 61–76.

13 I. v. Golosovsky, G. Salazar-Alvarez, A. López-Ortega, M. A. González, J. Sort, M. Estrader, S. Suriñach, M. D. Baró and J. Nogués, *Phys. Rev. Lett.*, 2009, **102**, 247201.

14 G. Salazar-Alvarez, J. Sort, S. Suriñach, M. D. Baró and J. Nogués, *J. Am. Chem. Soc.*, 2007, **129**, 9102–9108.

15 E. Lima, E. L. Winkler, D. Tobia, H. E. Troiani, R. D. Zysler, E. Agostinelli and D. Fiorani, *Chem. Mater.*, 2012, **24**, 512–516.

16 K. Sartori, G. Cotin, C. Bouillet, V. Halté, S. Bégin-Colin, F. Choueikani and B. P. Pichon, *Nanoscale*, 2019, **11**, 12946–12958.

17 N. Flores-Martinez, G. Franceschin, T. Gaudisson, S. Haj-Khlifa, S. G. Derouich, N. Yaacoub, J.-M. Grenèche, N. Menguy, R. Valenzuela and S. Ammar, *Sci. Rep.*, 2019, **9**, 19468.

18 M. A. Almessiere, Y. Slimani and A. Baykal, *J. Alloys Compd.*, 2018, **767**, 966–975.

19 N. A. Algarou, Y. Slimani, M. A. Almessiere, A. Baykal, S. Guner, A. Manikandan and I. Ercan, *J. Magn. Magn. Mater.*, 2020, **499**, 166308.

20 N. A. Algarou, Y. Slimani, M. A. Almessiere, F. S. Alahmari, M. G. Vakhitov, D. S. Klygach, S. V. Trukhanov, A. V. Trukhanov and A. Baykal, *J. Mater. Res. Technol.*, 2020, **9**, 5858–5870.

21 M. Vasilakaki, G. Margaris, E. Eftaxias and K. N. Trohidou, *Sci. Rep.*, 2015, **5**, 9609.

22 M. Vasilakaki, G. Margaris, E. Eftaxias, and K. N. Trohidou, *Exchange Bias from Thin Film to Nanogranular and Bulk Systems*, CRC Press, Taylor & Francis Group, Boca Raton, FL, 1st edn, 2017, vol. 1, ch. 6.

23 X. He, Y. Xu, X. Yao, C. Zhang, Y. Pu, X. Wang, W. Mao, Y. Du and W. Zhong, *RSC Adv.*, 2019, **9**, 30195–30206.

24 F. G. Silva, J. Depeyrot, Yu. L. Raikher, V. I. Stepanov, I. S. Poperechny, R. Aquino, G. Ballon, J. Geshev, E. Dubois and R. Perzynski, *Sci. Rep.*, 2021, **11**, 5474.

25 L. del Bianco, D. Fiorani, A. Testa, E. Bonetti and L. Signorini, *Phys. Rev. B: Condens. Matter Mater. Phys.*, 2004, **70**, 052401.

26 V. Narayanaswamy, I. A. Al-Omari, A. S. Kamzin, B. Issa and I. M. Obaidat, *Nanomaterials*, 2022, **12**, 262.

27 G. C. Lavorato, D. Peddis, E. Lima, H. E. Troiani, E. Agostinelli, D. Fiorani, R. D. Zysler and E. L. Winkler, *J. Phys. Chem. C*, 2015, **119**, 15755–15762.

28 N. Domingo, D. Fiorani, A. M. Testa, C. Binns, S. Baker and J. Tejada, *J. Phys. D: Appl. Phys.*, 2008, **41**, 134009.

29 M. S. Andersson, R. Mathieu, S. S. Lee, P. S. Normile, G. Singh, P. Nordblad and J. A. de Toro, *Nanotechnology*, 2015, **26**, 475703.

30  F. G. da Silva, *Magnetical properties, surface disorder and Exchange bias of magnetic nanoparticle*, University of Brasília/Sorbonne Université, 2013.

31  R. Cabreira-Gomes, F. G. Silva, R. Aquino, P. Bonville, F. A. Tourinho, R. Perzynski and J. Depeyrot, *J. Magn. Magn. Mater.*, 2014, **368**, 409–414.

32  R. C. Gomes, F. G. da Silva, T. Q. Muniz, G. Gomide, V. Pilati, R. Aquino, J. Geshev, R. Perzynski and J. Depeyrot, *J. Alloys Compd.*, 2020, 153646.

33  T. J. Salez, M. Kouyaté, C. Filomeno, M. Bonetti, M. Roger, G. Demouchy, E. Dubois, R. Perzynski, A. Cēbers and S. Nakamae, *Nanoscale Adv.*, 2019, **1**, 2979–2989.

34  A. G. Leonel, A. A. P. Mansur, S. M. Carvalho, L. E. F. Outon, J. D. Ardisson, K. Krambrock and H. S. Mansur, *Nanoscale Adv.*, 2021, **3**, 1029–1046.

35  R. Cabreira Gomes, F. G. da Silva, T.-Q. Silva, G. Gomide, V. Pilati, R. Aquino, J. Geshev, R. Perzynski and J. Depeyrot, *J. Alloys Compd.*, 2020, **824**, 153646.

36  F. G. Silva, R. Aquino, F. A. Tourinho, V. I. Stepanov, Y. L. Raikher, R. Perzynski and J. Depeyrot, *J. Phys. D: Appl. Phys.*, 2013, **46**, 285003.

37  G. Margaris, K. N. Trohidou and J. Nogués, *Adv. Mater.*, 2012, **24**, 4331–4336.

38  G. Margaris, M. Vasilakaki, D. Peddis, K. N. Trohidou, S. Laureti, C. Binns, E. Agostinelli, D. Rinaldi, R. Mathieu and D. Fiorani, *Nanotechnology*, 2017, **28**, 035701.

39  R. Aquino, F. A. Tourinho, R. Itri, M. C. F. L. e Lara and J. Depeyrot, *J. Magn. Magn. Mater.*, 2002, **252**, 23–25.

40  J. A. Gomes, M. H. Sousa, F. A. Tourinho, R. Aquino, J. Depeyrot, E. Dubois and R. Perzynski, *J. Phys. Chem. C*, 2008, **112**, 6220–6227.